




Computational modeling and molecular dynamics simulations of mammalian cytoplasmic tyrosyl-tRNA synthetase and its complexes with substrates

Vladyslav O. Kravchuk^{a,b,*} , Oleksandr V. Savytskyi^a , Konstantin O. Odynets^a, Vasyli V. Mykuliak^{a,c}  and Alexander I. Kornelyuk^{a,c}

^aDepartment of Protein Engineering and Bioinformatics, Institute of Molecular Biology and Genetics, National Academy of Sciences of Ukraine, 150, Akademika Zabolotnogo Str., Kyiv, 03143, Ukraine; ^bDepartment of Biotechnology, National Aviation University, 1, Kosmonavta Komarova Str., Kyiv, 03058, Ukraine; ^cInstitute of High Technologies, Taras Shevchenko National University of Kyiv, 64, Volodymyrs'ka Str., Kyiv, 01601, Ukraine

Communicated by Ramaswamy H. Sarma

(Received 4 June 2016; accepted 6 September 2016)

Cytoplasmic tyrosyl-tRNA synthetase (TyrRS) is one of the key enzymes of protein biosynthesis. TyrRSs of pathogenic organisms have gained attention as potential targets for drug development. Identifying structural differences between various TyrRSs will facilitate the development of specific inhibitors for the TyrRSs of pathogenic organisms. However, there is a deficiency in structural data for mammalian cytoplasmic TyrRS in complexes with substrates. In this work, we constructed spatial structure of full-length *Bos taurus* TyrRS (*Bf*TyrRS) and its complexes with substrates using the set of computational modeling techniques. Special attention was paid to *Bf*TyrRS complexes with substrates [L-tyrosine, K⁺ and ATP:Mg²⁺] and intermediate products [tyrosyl-adenylate (Tyr-AMP), K⁺ and PP_i:Mg²⁺] with the different catalytic loop conformations. In order to analyze their dynamical properties, we performed 100 ns of molecular dynamics (MD) simulations. MD simulations revealed new structural data concerning the tyrosine activation reaction in mammalian TyrRS. Formation of strong interaction between Lys154 and γ -phosphate suggests the additional role of CP1 insertion as an important factor for ATP binding. The presence of a potassium-binding pocket within the active site of mammalian TyrRS compensates the absence of the second lysine in the KMSKS motif. Our data provide new details concerning a role of K⁺ ions at different stages of the first step of the tyrosylation reaction, including the coordination of substrates and involvement in the PP_i releasing. The results of this work suggest that differences between ATP-binding sites of mammalian and bacterial TyrRSs are meaningful and could be exploited in the drug design.

Keywords: aminoacyl-tRNA synthetase; ATP; KMSKS; molecular modeling and dynamics; docking; MolDynGrid

1. Introduction

Aminoacyl-tRNA synthetases (aaRSs) are universal proteins that play an important role in translation of the genetic code. Tyrosyl-tRNA synthetase is the subclass Ic aaRS enzyme, which catalyzes the attachment of L-tyrosine to the 3' terminus of the cognate tRNA^{Tyr} at the preribosomal step of protein synthesis. The aminoacylation reaction consists of two steps. At the first step, the L-tyrosine is activated by ATP, forming the enzyme-bound Tyr-AMP intermediate and releasing the diphosphate ion (PP_i). At the second step of the reaction, the activated L-tyrosine is transferred to tRNA^{Tyr} to form the tyrosyl-tRNA^{Tyr} (Abergel, Rudinger-Thirion, Giege, & Claverie, 2007; Bedouelle, 1990; Bonnefond, Giegé, & Rudinger-Thirion, 2005; Kornelyuk, 1998).

In TyrRS, the described reaction occurs in the catalytic Rossmann-fold domain (Figure 1(A)). The class I aaRSs contain two conservative catalytic motifs having

signature “HIGH” and “KMSKS” sequences (⁴⁹HVAY⁵² and ²²²KMSSS²²⁶ in case of mammalian TyrRS), which take part at the first step of the reaction (Figures 1(A), and 2(A)). These motifs facilitate ATP binding and allow stabilization of the transition state (Yaremchuk, Krikliivyi, Tukalo, & Cusack, 2002). A catalytic KMSKS loop adopts different conformational states, which are usually described as open, semi-open, and closed (Kobayashi et al., 2005; Mykuliak, Dragan, & Kornelyuk, 2014). Recently, Datt and Sharma proposed reclassification of the three states into only two: extended and compact depending of distance between the KMSKS motif and the Rossmann fold (Datt & Sharma, 2014). In the crystal structures of human cytoplasmic TyrRS (*Hs*TyrRS) Protein Data Bank (PDB) IDs: 1N3L, 1Q11, 4QBT and 4Q93, the KMSKS motif's coordinates are missing.

Recent *in silico* study of *Mycobacterium tuberculosis* TyrRS (*Mt*TyrRS) revealed that the compact state of the

*Corresponding author. Email: v.o.kravchuk@imbg.org.ua

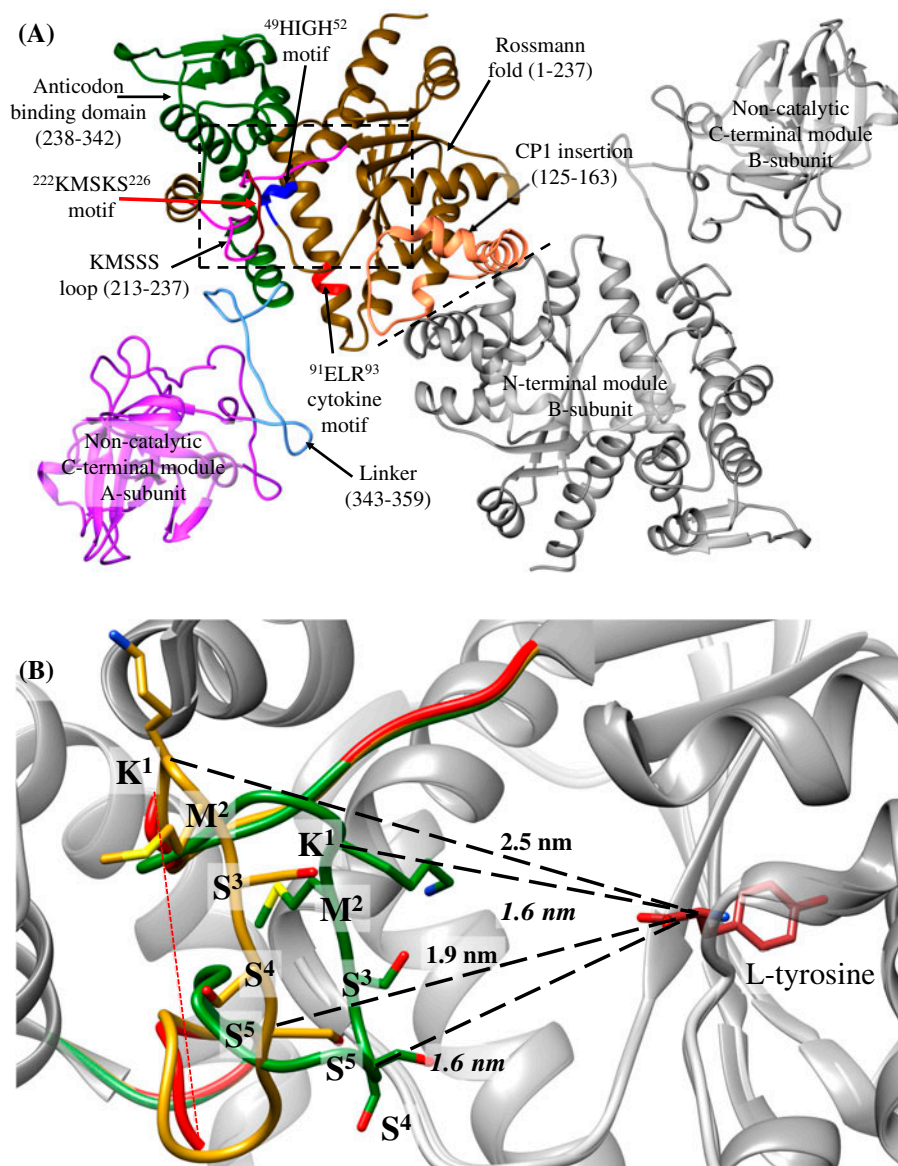


Figure 1. The structural elements of the modeled full-length *BtTyrRS*. A. The catalytic domain is in dark-gold, the anticodon-binding domain is in green and the C-terminal domain is in magenta. Interdomain linker is in light-blue. The KMSKS motif and the catalytic loop are in brown and pink, respectively, the HIGH motif is in blue, the ELR motif is in red. Dashed line shows an approximate interface between two N-terminal domains. TyrRS has no editing activity and contains only one (synthetic) active site per one subunit. Rectangle shows region engaged in section B. B. Superposition of N-terminal domains of *BtTyrRS* with the compact and extended conformation of the catalytic KMSSS loop and *HsTyrRS* (PDB ID: 1N3L). Only catalytic loops are colored in different colors. The catalytic loop with “gap” from 1N3L is in red, the extended and compact loops of *BtTyrRS* are in yellow and green, respectively. The distances between the C_α atoms of L-tyrosine and K¹ and S⁵ (from KMSKS motif) are shown in italic bold for the compact conformation and simple bold for the extended conformation. Hydrogen atoms are removed in all figures for clarity.

catalytic loop is stabilized by dynamic formation of two short antiparallel β -sheets at its flanking ends which hold the KMSKS-motif inside the active site (Mykuliak et al., 2014). In this work, we also investigated behavior of some disordered regions in the catalytic domain of *BtTyrRS*, i.e. the catalytic loop and the Val153–His158

disordered region of the connecting polypeptide 1 (CP1) (Figures 1(A) and 1(B)). It is necessary to note, that mammalian TyrRSs are K⁺ depending enzymes; K⁺ functionally replaces the second lysine of the KMSKS signature sequence (Austin & First, 2002b; Naidenov, Vudmaska, & Matsuka, 2001).

Table 1. The modeled structures and complexes of full-length *Bt*TyrRS.

<i>Bt</i> TyrRS structure	Abbreviation	KMSSS loop conformation	Occupancy of the active site	MD simulations time (ns)
1	<i>Bt</i> TyrRS _{Ex}	Extended	–	–
2	<i>Bt</i> TyrRS _{Cm}	Compact	–	100
3	<i>Bt</i> TyrRS ^{Tyr}	Compact	Tyr and K ⁺	–
4	<i>Bt</i> TyrRS ^{ATP+Tyr}	Compact	Tyr, K ⁺ and ATP:Mg ²⁺	100
5	<i>Bt</i> TyrRS ^{Tyr-AMP}	Compact	Tyr-AMP and K ⁺	–
6	<i>Bt</i> TyrRS _{Cm} ^{Tyr-AMP+PPi}	Compact	Tyr-AMP, K ⁺ and PP _i :Mg ²⁺	100
7	<i>Bt</i> TyrRS _{Ex} ^{Tyr-AMP+PPi}	Extended	Tyr-AMP, K ⁺ and PP _i :Mg ²⁺	20

Note: Tyr-AMP – tyrosyl-adenylate, ATP:Mg²⁺ – adenosine-5'-triphosphate coordinated by Mg²⁺ ion, PP_i:Mg²⁺ – inorganic diphosphate ion coordinated by Mg²⁺.

Structural studies of mammalian TyrRS have not only fundamental, but also biomedical significance. It was revealed that Charcot–Marie–Tooth disorder (CMT) (Dominant Intermediate CMT disorder type C) may be related to Gly41Arg and Glu196Lys point mutations and Val153–Val156 deletion in human TyrRS (Jordanova et al., 2006). In order to determine consequences of these mutations, it is necessary to identify their influences on the *Hs*TyrRS structure and conformational dynamics (Savytskyi & Kornelyuk, 2015). Moreover, TyrRS is an attractive therapeutic target for finding novel antibacterial agents (Chen et al., 2016; Xiao et al., 2015). Identifying differences in the catalytic mechanisms of bacterial and mammalian TyrRSs will facilitate the development of antibiotics that selectively target the bacterial TyrRS (Austin & First, 2002b). However, there are only few structural data for mammalian TyrRS comparing to the corresponding data for bacterial enzymes (Kobayashi et al., 2005).

The crystal structure of the full-length mammalian TyrRS is not currently available. Moreover, there are no crystal structures of the *Hs*TyrRS complexes with substrates (except L-tyrosine) even for its catalytic core structure without C-terminal domain (mini-*Hs*TyrRS). Therefore, it is relevant to use computational modeling and molecular dynamics (MD) for the mammalian TyrRS study. Previously, the structural modeling and MD techniques were applied for the full-length *Hs*TyrRS structure modeling (Savytskyi, Yesylevskyy, & Kornelyuk, 2013; Yesylevskyy, Savytskyi, Odynets, & Kornelyuk, 2011). It was established, that the ELR motif (Glu91, Leu92, Arg93) is responsible for interleukin-8-like cytokine activity of mini-*Hs*TyrRS (Wakasugi & Schimmel, 1999a, 1999b); C-terminal domains also have cytokine activity (Kornelyuk, Tas, Dubrovsky, & Murray, 1999; Wakasugi & Schimmel, 1999a, 1999b). Using the MD method in the 100 ns time interval, it was shown that full-length *Hs*TyrRS forms compact structure between N-terminal and C-terminal domains, which may protect the ELR cytokine motif (Savytskyi et al., 2013; Yesylevskyy et al., 2011).

Modern MD simulations are widely used in order to explore conformational flexibility and mechanism of enzymes (Hanoian, Liu, Hammes-Schiffer, & Benkovic,

2015; Swiderek, Tunon, Moliner, & Bertran, 2015), especially for aminoacyl-tRNA synthetases (Budiman, Knaggs, Fetrow, & Alexander, 2007; Li, Macnamara, Leuchter, Alexander, & Cho, 2015; Strom, Fehling, Bhattacharyya, & Hati, 2014). Substrate-induced conformational changes are responsible for the specific binding of substrates by enzymes. Previously, by fluorescent spectroscopy investigation of *Bt*TyrRS, it was revealed conformational changes induced by Tyr-AMP formation (Kornelyuk, Klimenko, & Odynets, 1995). In this work, we performed computational modeling and MD simulations of the *Bt*TyrRS structure and its complexes with substrates (Table 1).

2. Materials and methods

Full-length amino acid sequences of *Bos taurus* and *Homo sapiens* TyrRSs were used from the NCBI Gene database (<https://www.ncbi.nlm.nih.gov/protein/>) with identification numbers DAA32266.1 and NP_003671.1, respectively. The three-dimensional crystal structures were obtained from RCSB PDB archive. Visualization of macromolecules was performed using UCSF Chimera 1.10.2 (Pettersen et al., 2004) and Maestro 10.3 (Schrödinger, LLC, New York, 2015) packages.

2.1. Modeling of full-length *Bt*TyrRS_{Ex} structure

For building the full-length *Bt*TyrRS_{Ex} structure, previously reported the full-length *Hs*TyrRS structure (Savytskyi et al., 2013; Yesylevskyy et al., 2011) was used as the template due to their high similarity (95% sequence identity; 98% sequence similarity) (Figure 2(A)). The structure of the full-length *Hs*TyrRS dimer was constructed from the crystal structures of its N-terminal and C-terminal domains (PDB IDs: 1N3L:A, residues Ala3–Pro342 (Yang, Skene, McRee, & Schimmel, 2002) and 1NTG:A, residues Pro360–Ser528 (Yang, Liu, Skene, McRee, & Schimmel, 2003), respectively) using Modeller 9.7 software (Eswar et al., 2006; Martí-Renom et al., 2000). Missing N-terminal residues M1–D3, the residues K222–E228 of the catalytic loop and the linker residues D343–E359 were added using loops reconstruction option

(A)	<i>Bt</i> TyrRS	MGDSLSPPEEKLSLITRNLQEVLGEEKLKEILKERELK VW GTA TTG KP HVAY FVPMSKIADFLKAG	66	
	<i>Hs</i> TyrRS	MGDA PS PEEK HL ITRNLQEVLGEEKLKEILKERELK IY GTA TTG KP HVAY FVPMSKIADFLKAG	66	
	<i>Bt</i> TyrRS	CEVTILFADLHAYLDNMKAPWELLE LE RTSYENVIKAMLESIGVPLEK LR FIKGTDYQLSKEYITLD	132	
	<i>Hs</i> TyrRS	CEVTILFADLHAYLDNMKAPWELLE LR RTSYENVIKAMLESIGVPLEK KR FIKGTDYQLSKEYITLD	132	
	<i>Bt</i> TyrRS	VYRLSSVV Q HD AK KAGAEVVKQVEHPLLSGLLY Y PGL Q ALDEEYLKVDA Q FG GV D Q RK I PTFAEKY	198	
	<i>Hs</i> TyrRS	VYRLSSVV Q HD SK KAGAEVVKQVEHPLLSGLLY Y PGL Q ALDEEYLKVDA Q FG GI D Q RK I PTFAEKY	198	
	<i>Bt</i> TyrRS	LPALGYSKR I HLMN F MP V PGLTGS KMSS SEESKIDLLDRKEDVKKLKKAFCEPGNVNNGV L AFI	264	
	<i>Hs</i> TyrRS	LPALGYSKR V HLMN F MP V PGLTGS KMSS SEESKIDLLDRKEDVKKLKKAFCEPGNVNNGV L SFI	264	
	<i>Bt</i> TyrRS	RHVLFP L KSEFVILRDEKWGGNKTYTAY L DLEKDFAEV V HPGDLKNSVEVALNKLDP I REKFNT	330	
	<i>Hs</i> TyrRS	RHVLFP L KSEFVILRDEKWGGNKTYTAY V DLEKDFAEV V HPGDLKNSVEVALNKLDP I REKFNT	330	
	<i>Bt</i> TyrRS	PALKKLSAA Y PDPSK O K P AV K GP A KNSEPEEVI P SR L DI R VG K V IS V D K HPDADSLYVEKIDVGE	396	
	<i>Hs</i> TyrRS	PALKK L AA Y PDPSK O K P MA K GP A KNSEPEEVI P SR L DI R VG K I IT V E K HPDADSLYVEKIDVGE	396	
	<i>Bt</i> TyrRS	AE P RT V SVGLV Q FVPKEEL Q DR L VV L CVL N LP Q K M RG V ES Q GM L LCAS V EG V NR K VE P LD P PAGSA	462	
	<i>Hs</i> TyrRS	AE P RT V SVGLV Q FVPKEEL Q DR L VV L CVL N LP Q K M RG V ES Q GM L LCAS I EG I NR Q VE P LD P PAGSA	462	
	<i>Bt</i> TyrRS	PGER V FVKGYEK Q PD E EL K PK K V F E K LQ A DF K IS D E Y IA Q W K OT N FM T KL G S V SC S KL G GN I S	528	
	<i>Hs</i> TyrRS	PGE H V F V K GYEK Q PD E EL K PK K V F E K LQ A DF K IS E C I A Q W K OT N FM T KL G S I SC S KL G GN I S	528	
(B)	Enzyme	PDB ID	Substrate	Sequence
	<i>Pf</i> TyrRS*	3VGJ	Tyr-AMP	²³⁹ PGLLEGQEKMSKSDENSAI ²⁵⁷
	<i>Hs</i> TyrRS	1N3L	-	²¹⁶ PGLTGS--KMSSEESKI ²³²
	<i>Bt</i> TyrRS	-	-	²¹⁶ PGLTGS--KMSSEESKI ²³²
	<i>Hs</i> TrpRS	2QUI	ATP+Trp analog	³⁴¹ PALQGAQT KMSASDPNSSI ³⁵⁹
	<i>Mt</i> TyrRS	2JAN	-	²²⁵ TAADGT--KFGKSTGGGSL ²⁴¹

Figure 2. Amino acid sequence comparison. A. Amino acid sequence alignment of the bovine and human cytoplasmic TyrRSs. Differences between residues are colored in bold black while the active site residues (http://www.ncbi.nlm.nih.gov/protein/NP_003671.1) are colored in red. The catalytic HIGH, KMSKS and cytokine ELR motifs are underlined. B. Multiple amino acid sequence alignment of the remodeling fragment of the catalytic loop. *Hs*TrpRS and *Pf*TyrRS were considered as two alternative structural templates since they contain the compact KMSKS loop conformation. In result, *Pf*TyrRS was used for the catalytic loop remodeling. The fragment from the bacterial TyrRS is shown to represent the sequence difference.

in Modeller 9.7 (Fiser, Do, & Šali, 2000). The best structures were selected from each ensemble using the DOPE and MOF scores (Shen & Sali, 2006).

The Python script (*mutate_model.py*) in Modeller 9.15 was used to introduce 26 residue substitutions into full-length *Hs*TyrRS for both subunits (Figure 2(A)). For the obtained *Bt*TyrRS structure, addition of protocol hydrogen atoms and energy minimization using steepest descent and conjugated gradients algorithms were applied in UCSF Chimera 1.10.2 package. All structures were verified using the MolProbity web server (Chen et al., 2009). The structure of mini-*Bt*TyrRS was obtained from previously described full-length *Bt*TyrRS by deletion of both C-terminal domains.

2.2. Modeling of compact KMSKS loop conformation

The compact catalytic loop modeling was performed using Modeller 9.15 software. We modeled two alternative catalytic loops on base of the different templates: *Plasmodium falciparum* TyrRS (*Pf*TyrRS, PDB ID: 3VGJ) (Bhatt et al., 2011) and human tryptophanyl-tRNA synthetase (*Hs*TrpRS, PDB ID: 2QUI) (Shen et al., 2008). However, catalytic loop based on *Pf*TyrRS was used for further analysis. Initial crystal structure template (1N3L) had extended catalytic loop conformation with seven ²²²KMSSE²²⁸ residues missed. We deleted and remodeled 15 residues in each subunit between Pro216 and Ile232 (accounting two short

deletions) in both subunits of *Bt*TyrRS_{Ex} (Figure 2(B)). In result, we obtained *Bt*TyrRS_{Cm} (Figure 1(B)).

2.3. Modeling of *Bt*TyrRS^{Tyr} and *Bt*TyrRS^{ATP+Tyr} Complexes

*Bt*TyrRS^{Tyr} complex was constructed using protein-protein superposition of *Bt*TyrRS_{Cm} and mini-*Hs*TyrRS in complex with L-tyrosine and K⁺ (PDB ID: 4QBT) (Sajish & Schimmel, 2015) keeping *Bt*TyrRS_{Cm} with K⁺ and the L-tyrosine substrate from 4QBT. Superposition of both structures was done using PyMOL 1.7.0 software (Schroödinger, LLC).

*Bt*TyrRS^{Tyr} complex was used as a receptor for *Bt*TyrRS^{ATP+Tyr} complex modeling. The ATP:Mg²⁺ conformation was used from *Geobacillus stearothermophilus* TrpRS (*Gs*TrpRS, PDB ID: 1MAU) (Retailleau et al., 2003). Before molecular docking processing, protocol hydrogen atoms were added to the ATP molecule using Chimera software. ATP:Mg²⁺ and other substrates were docked only into subunit A leaving subunit B in a substrate-free state. AutoDock 4.2.6 (Morris et al., 2009) software was used for molecular docking. Rigid typical ATP:Mg²⁺ conformation was docked into flexible active site of *Bt*TyrRS with 12 flexible residues: Trp40, Thr42, His49, Tyr52, Val54, Asn212, Val215, Lys222, Met223, Ser224, Ser225 and Ser226. All these residues surround ATP in initial approximate complex constructed by *Bt*TyrRS^{Tyr} and *Gs*TrpRS superposition (Figure 3).

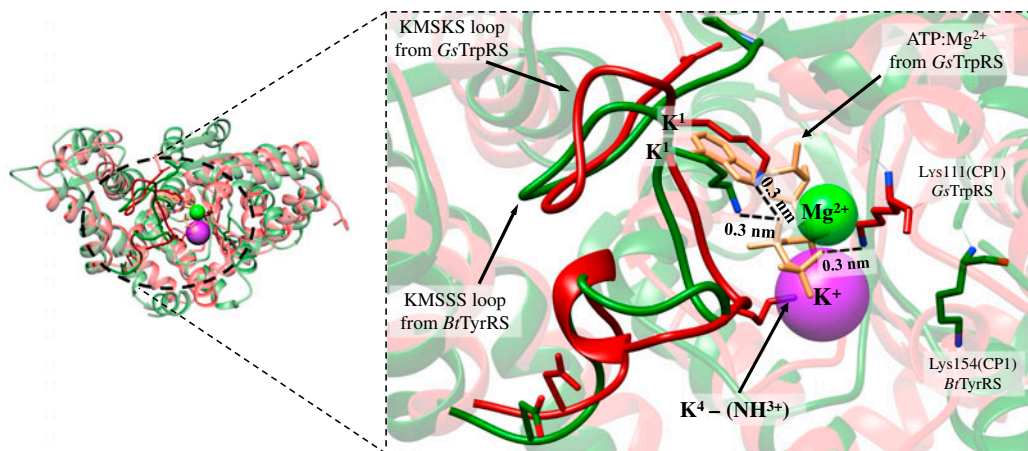


Figure 3. Superposition of N-terminal domains of *BtTyrRS*^{Tyr} (green) and *GsTrpRS* (PDB ID: 1MAU) (red) complexed with ATP: Mg²⁺ and Trp analogue. The active site and catalytic loop regions are zoomed. Superposition reveals same spatial position of the NH₃⁺-group of the second lysine (K⁴) from the KMSKS motif and the K⁺ ion. Both K¹ from the different loops have the same distance to the O_{1B} atom of ATP. Due to these factors, the superposition of 1MAU and *BtTyrRS* can be used to determine an approximate position of the ATP molecule in *BtTyrRS* regarding the catalytic loop and the K⁺ ion. Lys111 of 1MAU, which corresponds to Lys154 in *BtTyrRS* and *HsTyrRS*, forms hydrogen bond with γ -phosphate in the crystal structure of *GsTrpRS* while Lys154 is located about 0.9 nm relatively ATP.

The subunit's A active site was placed into grid box centering on HIGH i KMSKS motifs. The grid size was set to 40 × 40 × 40 points with grid spacing 0.0375 nm. We set such relatively small grid box to decrease degrees of freedom and provide maximum accuracy of docking results. The Mg²⁺ and K⁺ ions used AMBER force field potentials as defined in the AutoDock software. We assigned partial charges of ions manually as we found that AutoDock automatically set them to neutral. Lamarckian genetic algorithm (Morris et al., 1998) was chosen for these studies because results of others (Chen et al., 2007) indicated this as one of the most efficient and robust algorithm for ligand-bound metal ions in docking of small ligands. A maximum number of energy evaluations parameter was set to 300,000 with a population size 150. Several conformations with the lowest binding energy were selected for further analysis.

2.4. Modeling of *BtTyrRS*^{Tyr-AMP} and *BtTyrRS*^{Tyr-AMP+PPi} complexes

Structural coordinates of mammalian TyrRS in complex with Tyr-AMP intermediate are still unknown. To construct such complex, we attempted to carry out docking of flexible Tyr-AMP into flexible *BtTyrRS* active site. Unfortunately, this attempt was unsuccessful, since AutoDock has a torsional number limit (32 torsions maximum). Even with torsional optimizations, results were unsatisfactory. Thus, we carried out docking of rigid Tyr-AMP into flexible active site.

There are several TyrRS crystal structures with intermediate product or its analogue present, however, to obtain complex with the most accurate Tyr-AMP position and con-

formation we used following approach. Firstly, we constructed approximate mini-*BtTyrRS* complex with Tyr-AMP and K⁺ ion. For its construction, the atomic coordinates of tyrosine moiety of Tyr-AMP from *PfTyrRS* (PDB ID: 3VGJ) were superimposed on the L-tyrosine substrate which located in *BtTyrRS*^{Tyr} (extended catalytic loop conformation) using *pair fitting* function of PyMOL software. After coordinates superposition, the mini-*BtTyrRS*, K⁺, and Tyr-AMP were kept. Then, 100 ns MD simulations of mini-*BtTyrRS* complex with Tyr-AMP and K⁺ have been carried out to determine equilibrated Tyr-AMP conformation. Details concerning MD simulations are described in the next section. Thus, optimized Tyr-AMP conformation was used as rigid for further docking into flexible active site. *BtTyrRS*^{ATP+Tyr}, after removing all ligands except K⁺, was used as a receptor with conformation of the active site optimized for ATP and Tyr moieties. Tyr39, Trp40, Thr42, and His49 residues were set as flexible with all torsions kept. Docking conditions were the same as previously except grid box size (64 × 42 × 40) and energy evaluations (700,000). One conformation with the lowest binding energy was selected for further analysis.

*BtTyrRS*_{Cm}^{Tyr-AMP+PPi} complex was constructed by *BtTyrRS*^{Tyr-AMP} and *BtTyrRS*^{ATP+Tyr} complexes superposition, keeping *BtTyrRS*^{Tyr-AMP} and PP_i:Mg²⁺. Additional *BtTyrRS*_{Ex}^{Tyr-AMP+PPi} with *extended* catalytic loop conformation was also constructed by the molecular docking method with the same parameters. Since the *BtTyrRS*_{Ex} with *extended* catalytic loop conformation was used as a receptor—Tyr39, Trp40, Tyr52, Val54, Asp173, and Asp187 were set as flexible residues with all torsions kept. Addition of PP_i:Mg²⁺ was performed by the same instruction.

2.5. MD simulations

Obtained different systems of mini-*BtTyrRS* (see 2.4) and full-length *BtTyrRS* (Table 1) were simulated for 100 ns time interval using all-atom MD simulations with GROMACS 5.0 package (Páll, Abraham, Kutzner, Hess, & Lindahl, 2015; Van Der Spoel et al., 2005). For all the simulations conducted, the CHARMM27 force field (Bjellmar, Larsson, Cuendet, Hess, & Lindahl, 2010) was used. Force field topologies for the ligands were prepared using SwissParam web server (Zoete, Cuendet, Grosdidier, & Michielin, 2011). We generated at least three trajectories for each system. Mini-*BtTyrRS* and full-length *BtTyrRS* were placed into rectangle boxes with dimensions $15.1 \times 14.1 \times 14.1$ nm and $18.0 \times 14.0 \times 13.0$ nm, respectively. The explicit TIP3P water molecules (Jorgensen & Madura, 1983) were added. All simulations were performed under periodic boundary conditions. In order to neutralize the overall charge of systems with mini-*BtTyrRS* complexes, four Na^+ ions were added. Systems with full-size *BtTyrRS* complexes were neutralized with K^+ and Cl^- counterions at 150-mM KCl salt concentration. Each system was energy minimized and then equilibrated with positioning restraints on heavy atoms of the protein before the MD simulations were initiated. The leap-frog integration algorithm was used, together with a 2.0 fs time step. All bond lengths were constrained using the LINCS algorithm (Hess, Bekker, Berendsen, & Fraaije, 1997). Long-range electrostatic interactions were computed using the fourth-order particle mesh Ewald (PME) method (Essmann et al., 1995) with a Fourier spacing of 0.16 nm. The real space coulombic interactions and the pair-list calculations were set to 1.0 nm for mini-*BtTyrRS* and 1.2 nm for full-length *BtTyrRS*. A twin-range cut-off of 1.0 nm for mini-*BtTyrRS* and 1.2 nm for full-length *BtTyrRS* was used for the van der Waals interactions. The temperature of 310 K and pressure of 1 atm were maintained by coupling temperature and pressure baths using the V-rescale (Bussi, Donadio, & Parrinello, 2007) and Parrinello–Rahman (Parrinello & Rahman, 1981) methods with relaxation times of 0.2 and 1.0 ps, respectively.

MD simulations have several well-known difficulties and limitations. Force fields are computational approximations; in other words, classical parameterization of non-classical effects. In classical MD, the effect of the electrons is approximated as a single potential energy surface. Such classical treatment of particle-particle interactions cannot reproduce chemical reactions. Also the partial charges in MD simulations are represented as static fixed charges that are located at the center of an atom and such electronic effects like charge transfer and polarization are predicted computationally. Researches of aaRS, with using of MD methods, also may face some challenges concerning the MD limitations (Kapustina &

Carter, 2006; Li et al., 2015). Finally, MD simulations require a lot of computational resources. However, this problem could be resolved to some extent using modern computer technologies (see Section 2.7).

2.6. MD trajectory analysis

MD trajectories analysis was performed in GROMACS software. The Root Mean Square Deviations (RMSD) and Root Mean Square Fluctuations (RMSF) were calculated using *gmx rms* and *gmx rmsf* routines, respectively. It is necessary to note that the difference between RMSD and RMSF is that with the latter the average is taken over time, giving a value for each C_α atom of a protein, whereas with RMSD the average is taken over all the C_α atoms, giving time-specific values. Hydrogen bonds were monitored with the *gmx hbond* routine. The *readHBmap* Python script (http://www.gromacs.org/Downloads/User_contributions/Other_software) was used to extract the hydrogen bond existences from HB Map file (.xpm) generated by *gmx hbond* routine from GROMACS 5.0. The average structure from the most populated cluster during MD simulations (MD simulated structure) was determined using *gmx cluster* routine with the gromos method (Daura et al., 1999) and 0.2 nm cut-offs. Visual analysis of MD trajectories was performed using VMD 1.9.2 software (Humphrey, Dalke, & Schulten, 1996).

2.7. Technical details

Molecular modeling, MD simulations, and data analysis were performed in the MolDynGrid Virtual Laboratory (VL) (<http://moldyngrid.org>) as a part of Ukrainian National Grid (UNG, <http://ung.in.ua>) and European Grid Infrastructure (EGI, <http://egi.eu>). MolDynGrid VL was established for interdisciplinary studies in computational structural biology, especially for extensive MD simulations of biological macromolecules and their complexes, which required a high processing power and immense storage space. It usually utilizes computing elements of 9 clusters and storage elements of 2 clusters that correspond to ~2500 CPUs and ~100 TBytes of disk space, respectively (Salnikov, Sliusar, Sudakov, Savytskyi, & Kornelyuk, 2009, 2010; Savytskyi, Sliusar, Yesylevskyy, Stirenko, & Kornelyuk, 2011; Yesylevskyy, 2015).

3. Results and discussion

In order to obtain the complexes and corresponding structural elements, we developed a specific modeling approach. In the result, seven *BtTyrRS* model structures (among them five with low molecular weight substrates and intermediates) with different conformations of the catalytic loop, which correspond to different catalytic

states of the catalytic reaction, were constructed. For the selected complexes, we performed MD simulations (Table 1). In this research, special attention was paid to dynamical behavior of the enzyme, which occurs at the first step of the catalytic reaction, namely upon the Tyr-AMP formation. The first part of this work is devoted to analysis of the modeled structures, while the second part is devoted to their dynamical characteristics.

3.1. Compact KMSSS loop conformation analysis

The catalytic loop bearing the KMSKS motif of TyrRS and plays the important role in the catalysis of the L-tyrosine activation step of reaction (Austin & First, 2002a; First & Fersht, 1995). Catalytic KMSKS loop connects the catalytic and the anticodon-binding domains and in the same time, it is a critical structural element of the active site in the whole class I aaRSs (Figures 1(A) and 1(B)). However, the role of the KMSKS motif in mammalian TyrRS is less expressed comparing to prokaryotic TyrRS (Austin & First, 2002a). To distinguish the mammalian catalytic loop without the second lysine residue, we annotated it as the KMSSS loop while the catalytic loop in general is annotated as a KMSKS loop. Each position of the motif's residue was numbered as $K^1 M^2 S^3 K^4(S^4) S^5$. Traditionally, three KMSKS loop conformational states are described as open, semi-open, and closed conformations (Li, Froeyen, & Herdewijn, 2008; Mykuliak et al., 2014). However, in recent work Datt and Sharma proposed reclassification of the three states into only two: extended and compact (Datt & Sharma, 2014). The authors also revealed the second lysine (K^4) presence in ~87% of the TyrRS structural and proteome-wide sequences. Because the KMSSS loop structure had been unknown it was not accounted during the Datt and Sharma analysis, however, we prefer to use such classification for mammalian TyrRS.

Before protein–ligand docking processing, it was necessary to perform structural modeling of compact KMSSS loop conformation since contacts between a catalytic loop and substrates are quite important (Austin & First, 2002a; First & Fersht, 1995). For compact KMSSS loop modeling, we considered two possible template structures: *Pf*TyrRS, PDB ID: 3VGJ (Bhatt et al., 2011) and *Hs*TrpRS, PDB ID: 2QUI (Shen et al., 2008). *Hs*TrpRS supposed to be a good template due to the absence of the second lysine residue in KMSKS motif (9/17 matches within the catalytic loop remodeling fragment (Figure 2(B)). Moreover, high homology of both these enzymes was indicated in other works (Doublé, Bricogne, Gilmore, & Carter Jr, 1995; Shen et al., 2008). However, two closely related subclass Ic aaRSs (TyrRS and TrpRS) have developed different strategies to compensate the missing second lysine residue in higher eukaryotes (Yang et al., 2007). Since K^+ ion plays role

of missing K^4 in *Hs*TyrRS (Austin & First, 2002b), we suggest that structure with both lysines is the most appropriate template for catalytic loop modeling. In contrast, the catalytic loop from *Mt*TyrRS has very low sequence homology (3/17 matches within the remodeling fragment). Thus, we chose *Pf*TyrRS, which is eukaryotic TyrRS with high level of the catalytic loop sequence identity comparing to the KMSSS loop (10/17 matches within the remodeling fragment) (Figure 2(B)).

Since mammalian TyrRS has critical substitution K^4/S^4 in the KMSKS motif, it is necessary to investigate its structural and functional consequences. The modeled compact KMSSS loop has similar conformation to other KMSKS loop. Superposition of the *Bt*TyrRS^{Tyr} and the *Gs*TrpRS monomers shows this structural similarity while the *Gs*TrpRS has not been used as a structural template for modeling (Figure 3). In spite of the KMSSS loop being shorter, the critical K^1 residues have the same (0.3 nm) distances between their NH_3^+ -groups and the ATP's O_{1B} oxygen atom (Figure 3). Among the catalytic loop residues, the position of KMSSS residues defines its conformational state. To compare the conformational states, distances from the C_α atoms of K^1 and S^5 to the L-tyrosine's C_α atom were calculated. The distances from K^1 at extended and compact conformations are 2.5 and 1.6 nm, respectively, while distances from S^5 at extended and compact conformations are 1.9 and 1.6 nm, respectively (Figure 2(B)). Dynamical behavior of the KMSSS loop is discussed in the next sections.

3.2. ATP:Mg²⁺ and Tyr-AMP localization in the active site

The aminoacylation reaction occurs under the presence of Mg^{2+} ion which is necessary to neutralize the four negative charges of ATP triphosphate group (Doublé, Bricogne, Gilmore, & Carter, 1995). To construct *Bt*TyrRS^{ATP+Tyr} complex, we carried out an analysis of all class I aaRSs crystal structures in which ATP presents in complex with Mg^{2+} (PDB IDs: 1J09, 1N75 (Sekine et al., 2003), 1M83, 1MAU (Retailleau et al., 2003), 1YID (Buddha & Crane, 2005) and 2QUI). It was revealed that ATP conformation in which Mg^{2+} coordinates all three phosphate groups is typical for class I aaRSs (Figure S1A–E). Analysis of these complexes also suggests that conformation of ATP:Mg²⁺ where Mg^{2+} coordinates all three phosphates of ATP is inherent for enzymes, which have both lysines in KMSKS motif. Since K^+ functionally replaces the absence of second lysine (K^4) in the KMSKS-like motif of *Hs*TyrRS (Austin & First, 2002b), we carried out superposition of the *Bt*TyrRS^{Tyr} and the *Gs*TrpRS (PDB ID: 1MAU) complexes to investigate their structural relation (Figure 3). As expected, superposition revealed the same spatial position of the K^4 —(NH_3^+) group and the K^+ ion.

Therefore, among present structures, we used the typical ATP:Mg²⁺ conformation from the most homologous to mammalian TyrRS – GsTrpRS (Retailleau et al., 2003) for protein–ligand docking (see Section 2.3). Also GsTrpRS is one of the most studied class I aaRSs in case of interactions between the enzyme and ATP:Mg²⁺ (Kapustina & Carter, 2006; Retailleau et al., 2003). Thus, among selected lowest binding energy conformations, we chose one, which satisfied following criteria: (1) presence of contacts with the HIGH and the KMSKS motifs; (2) imitation of the K⁴ position by the K⁺ ion relatively to the ATP molecule.

Before docking, the Tyr-AMP molecule was optimized by the method of MD simulations (see Section 2.4). Thus, Tyr-AMP localization was chosen on base of the lowest binding energy. In result, both AMP moieties of ATP and Tyr-AMP had similar location into the active site.

3.3. Dynamical behavior of modeled complexes

Based on RMSD analysis, the obtained MD simulations trajectories of *Bt*TyrRS could be divided into two parts: deviations calculated during the first ~50 ns (stabilization) and 50–100 ns (equilibrated state). Calculated C_α atoms' RMSD values demonstrate the global stability of the protein structure in the course of MD simulations with the deviation of 1.25, 1.5, and 1.6 nm for the full-length enzyme in *Bt*TyrRS_{Cm}, *Bt*TyrRS^{ATP+Tyr}, and *Bt*TyrRS_{Cm}^{Tyr-AMP+PPi}, respectively. In fact, the C-terminal domain and the interdomain linker have substantial impact on whole RMSD values. Therefore, the values were calculated for the separate N-terminal domains with residue numbers 1–342 and 529–870 for subunits A and B, respectively (Figure 4(A)). For the same systems but only for the two N-terminal domains, the deviations were 0.28, 0.35, and 0.28 nm, respectively (Figure 4(A)). RMSD values of *Bt*TyrRS are similar to those for *Hs*TyrRS (Savytskyi et al., 2013).

To monitor the changes in the “compactness” of the protein during the MD simulations, we calculated its radius of gyration (R_g) (Figure 4(B)). A decrease in R_g during the course of MD simulations indicates the structural changing from an elongated to a more globular protein structure. R_g for *Bt*TyrRS^{ATP+Tyr} and *Bt*TyrRS_{Cm}^{Tyr-AMP+PPi} decreased after ~25 ns from 4.3 to 4.2 and 3.4 nm, respectively, and for the separate N-terminal domains stable values were 3.45 and 3.54 nm, respectively. R_g of the substrate-free enzyme was decreasing during 0–90 ns and then stabilized (Figure 4(B)). The full-length *Bt*TyrRS_{Cm}^{Tyr-AMP+PPi} and *Bt*TyrRS_{Cm} show lower R_g values comparing to *Bt*TyrRS^{ATP+Tyr} with difference ~0.5 nm. These data support the idea that TyrRS in solution consists of a number of asymmetric conformations with different degree of compactness (Savytskyi

et al., 2013; Yesylevskyy et al., 2011). C-terminal domain and interdomain linker also influence on R_g values, so they were calculated for N-terminal domains separately. N-terminal domains of *Bt*TyrRS_{Cm}^{Tyr-AMP+PPi} show less compactness comparing to *Bt*TyrRS^{ATP+Tyr} and *Bt*TyrRS_{Cm}. These data assume that the presence of both Tyr-AMP and PP_i induces decreasing of the catalytic domain's compactness and will be discussed in details in the next sections.

The RMSF values of C_α atoms for N-terminal domains were analyzed at equilibrated state at 50–100 ns time interval (Figure 4(C)). The flexible linkers and C-terminal domains were omitted because of the reason described before. This analysis revealed enhanced fluctuations of the KMSSS loop and the CP1 insertion loop (Val153–His158). According to these data, the KMSSS loop may either maintain compact conformation during whole simulation time or adopt an extended conformation from the compact one in different *Bt*TyrRS_{Cm} trajectories. Therefore, the KMSSS loop may have either low or very high fluctuations in a substrate-free state of the enzyme (Figure 4(C), Video S1). To compare these different KMSSS loop conformations adopted after MD simulations with *Hs*TyrRS crystal structure (PDB ID: 4QBT), we superimposed them (Figure S2). If to remove residues between Glu220 and Lys231, i.e. missing in 4QBT, both loops will look quite similar to each other (Figure S2). Taking together, these data suggest that substrate-free (or only with L-tyrosine) mammalian TyrRS consists of the structures with different KMSSS loop conformations. Therefore, coordinates of KMSKS motif are missed in the *Hs*TyrRS crystal structures. This result is in good agreement with the Datt and Sharma analysis of TyrRS in which ATP binding pocket is not occupied (Datt & Sharma, 2014). In recent research of *Mt*TyrRS, it was suggested that formation of two short antiparallel β -sheets (before and after KMSKS motif) may stabilize catalytic loop holding KMSKS motif inside the active site (Mykuliak et al., 2014). In this work, we also noticed only one similar β -sheet (before KMSKS motif) formation in *Bt*TyrRS but less expressed (Video S1). While in every crystal of mammalian TyrRS the catalytic loop structure is not full (at least seven residues are missing), the majority of bacterial TyrRS structures contain the whole structure even without substrate presence. Thus, we suggest that the catalytic loop in bacterial TyrRS may be much more rigid than in mammalian TyrRS. This suggestion supports the experimental study which stated that the role of KMSKS motif is less expressed in mammalian TyrRS comparing to bacterial TyrRS (Austin & First, 2002a).

3.4. Interactions between the active site and ATP/Tyr-AMP

Hydrogen bonds between the *Bt*TyrRS active site residues and ATP/Tyr-AMP revealed by MD simulations are

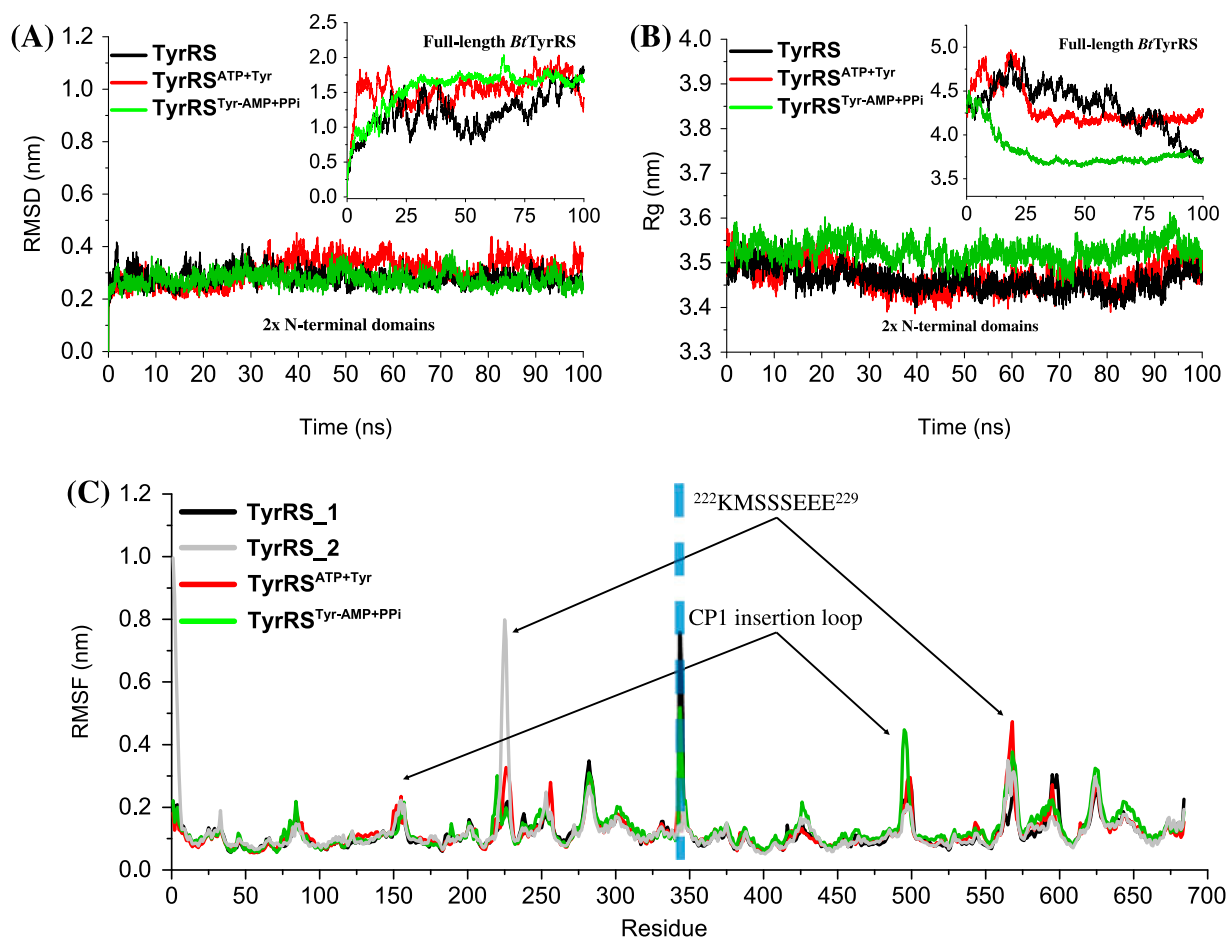


Figure 4. Dynamical characteristics of the modeled *BfTyrRS* complexes. The full-length enzyme contains 2x528 aa while one N-terminal domain 342 aa. A. RMSD plots of the C α atoms from the starting structure during MD simulations. In case of full-length enzyme, values show global stability for both complexes after 50 ns of simulation time. Equilibration of full-length enzyme significantly depends from linker and C-terminal module behavior. Values for core of N-terminal domains show stability of the catalytic core during MD simulations. B. Radius of gyration of the *BfTyrRS* complexes during 100 ns of MD simulations. Values for the full-length enzyme are different because there are no unique binding interfaces between N- and C-terminal domains. N-terminal domains of *BfTyrRS*^{Tyr-AMP+PPi} complex are slightly less compact comparing to other. C. RMSF plots of the C α atoms after equilibration (MD simulation time 50–100 ns). Discontinuous blue line is distinguishing different subunits. The regions of the KMSSE and CP1 insertion loops are pointed in the graph. ²²²KMSSEEE²²⁹ residues, coordinates of which are missed in every *HsTyrRS* crystal structure, may adopt different conformational states in different *BfTyrRS*_{Cm} trajectories. Changing of conformational state is accompanied by high RMSF values. The other RMSF peaks correspond to the unstructured regions located within N-terminal domain.

listed in Table 2. Residues of the KMSKS motif form hydrogen bonds with ATP. Lys222 (K¹) is the donor of hydrogen and positive charge, impact of Lys222 is one of most significant in the ATP stabilization (Table 2). During MD simulations, K¹ has one of the lowest RMSF values and the strongest interaction with ATP among KMSSE residues (Figure 4(C), Table 2). Therefore, K¹ is one of the key factors that keep the KMSSE loop in the compact conformation during whole simulations time of *BfTyrRS*^{ATP+Tyr} complex.

In order to investigate conformational changes of the active site, ligands' surrounding with cut-off 0.4 nm were compared between the initial and MD simulated

structures. In the initial *BfTyrRS*^{ATP+Tyr} complex within 0.4 nm of ATP molecule 19 residues (9 hydrophobic, 3 hydrophilic, 6 polar and 1 charged) were located, while in the MD-simulated structure within the same radius 20 residues (10 hydrophobic, 2 hydrophilic, 6 polar and 2 charged) were located. In the initial structure, the ATP forms hydrogen bonds with Trp40, Lys222, Ser224, Ser226 and L-tyrosine, while in the MD-simulated structure with Trp40, Asn212, Val215, Lys222, Met223, Ser224, Ser225, Ser226, and Lys154 (Figure 5(A)).

Among *HsTyrRS* crystal structures, there are two of them in which potassium-binding pocket (Thr42, Ala43, Tyr52 and Tyr97) is occupied by K⁺ (Sajish &

Table 2. Hydrogen bonds formation in the *Bt*TyrRS complexes.

<i>Bt</i> TyrRS's atom	Substrate's atom	Lifetime (%)
	ATP	
Val215(NH)	N1	95.3
Asn212(ND2H1)	O2'	86.0
Trp40(NE1H)	O3'	84.5
Lys154(NZH1)	O1G	77.8
Lys222(NZH1)	O1B	62.2
Tyr52(OH)	O2B	56.3
Ser225(NH)	O2B	39.2
Met223(O)	H1N6	38.4
	Tyr-AMP	
Ala43(NH)	O2P	98.9
Thr42(OG1H)	O2P	98.6
Asp173(OD1)	HO	98.4
Tyr39(OH)	OH	97.2
Asn212(ND2H1)	O2'	77.1
Val215(NH)	N1	73.9
Trp40(NEH1)	O3'	63.3

Notes: Hydrogen bonds are listed between the substrates and the active site residues of *Bt*TyrRS. The bonds were analyzed within 50–100 ns of simulation time (equilibrated state), where lifetime is relation of frames in which hydrogen bond is present to the total number of frames and multiplied by 100%. Only hydrogen bonds with lifetime more than 30% and major atom pairs are listed.

Schimmel, 2015; Yang et al., 2003). Initially, localized K^+ ion had released from the active site during MD simulations and its place in potassium-binding pocket rapidly took another K^+ from the water-ion medium (Figure 5(A), Video S2). This effect was also noticed in *Hs*TyrRS (Savytskyi et al., manuscript in preparation) and is repeated in the *Bt*TyrRS system.

In the initial *Bt*TyrRS_{Cm}^{Tyr-AMP+PPi} complex, the Tyr-AMP intermediate forms hydrogen bonds with Trp40, Thr42, and Ala43, while in the MD-simulated structure with Tyr39, Trp40, Thr42, Asp173, Asn212, and Val215. Before MD simulation within 0.4 nm of the Tyr-AMP molecule 23 residues (12 hydrophobic, 3 hydrophilic, 6 polar and 2 charged) were located, while in the MD simulated structure within the same radius 23 residues (15 hydrophobic, 3 hydrophilic, 4 polar and 1 charged) were located (Figure 5(B)). In the course of MD simulations, both complexes were forming hydrogen bonds between the catalytic KMSSS loop (Val215 main-chain atoms) and adenosine ring of Tyr-AMP. In addition, Asn212 was forming hydrogen bond with 2'OH ribose moiety. These hydrogen bonds are typical for class I aaRSs (Kobayashi et al., 2005).

Thus, here we observed formation of a number of key interactions (hydrogen bonds which mentioned above) between the enzyme and ATP/Tyr-AMP molecules during MD simulations. It is not surprisingly that they were not predicted by the molecular docking method because the reference structure did not contain

both substrates (ATP and Tyr), which induce conformational changes of the enzyme. Therefore, we suggest that it is necessary to perform MD simulations for such systems after molecular docking.

3.5. New Role of CP1 insertion loop in mammalian TyrRS during Tyr-AMP formation

The catalytic Rossmann-fold domain of class I aaRSs contains an insertion, known as CP1 (Starzyk, Webster, & Schimmel, 1987). The CP1 insertion is found in all class I aaRS and, for some of them, contains the active site for editing mistakes during translation. In TyrRS, CP1 is small comparing to other class I enzymes and has no editing active site. However, TyrRS has recognition residues within CP1 for binding the acceptor stem of tRNA^{Tyr} and, in particular, the 39-aa peptide motif (Leu125–Gly163 for mammalian TyrRS) within CP1 is essential for discrimination of the first base pair C1:G72 of the acceptor stem (Naidenov, Vudmaska, Kornelyuk, & Matsuka, 2000; Wakasugi, Quinn, Tao, & Schimmel, 1998). It was suggested that disordered region of CP1 (CP1 insertion loop, namely Val153–His158) probably becomes ordered on binding to tRNA^{Tyr} (Yang et al., 2002). Our results suggest new function of this disordered region. During MD simulations Lys154, which is localized in this region, forms stable hydrogen bond with γ -phosphate of ATP (Table 2, Figure 5(A)). It is necessary to note, that Lys154 was not included in the set of flexible residues during molecular docking since it was located \sim 1.0 nm from γ -phosphate in the initial approximate complex (Figure 3). This result well correlates with the investigation of two CMT type C disease-associated *Hs*TyrRS mutants that display a substantial (>100-fold) decrease in the Tyr-AMP formation (Froelich & First, 2011). The first mutant form is Val153–Val156 deletion and the second one is Gly41Arg substitution. Thus, the probable reason for critical decreasing of catalytic activity in case of Val153–Val156 deletion is the direct loss of the important Lys154. Recent analyses of MD simulation trajectories of Gly41Arg mutant form of *Hs*TyrRS have shown the β -sheet formation in the region Lys147–Glu157 between helices H9 and H10 of CP1 insertion (Savytskyi & Kornelyuk, 2015). Thus, one of the reasons for decreasing of catalytic activity in case of Gly41Arg mutation could be the structural rearrangement of the Val153–His158 region that causes another localization of important Lys154.

In the case of the bacterial *Gs*TrpRS (PDB ID: 1MAU), it was revealed the important role of the analogous Lys111 residue (in CP1), which forms similar hydrogen bond with γ -phosphate of ATP (Kapustina & Carter, 2006; Retailleau et al., 2003). In *Gs*TrpRS 1MAU crystal, CP1 insertion is more ordered than in *Bt*TyrRS. Most likely, that in a large timescale it is

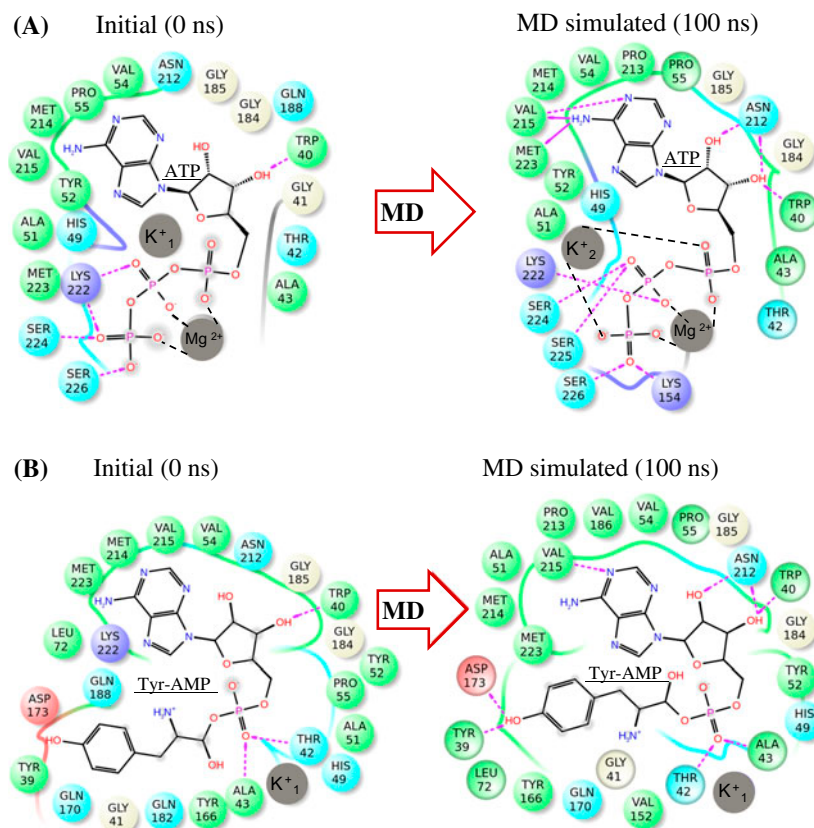


Figure 5. Localization of the initial and MD simulated ATP:Mg²⁺(A) and Tyr-AMP (B) ligands into the active site of *BtTyrRS*. Residues in cut-off 0.4 nm are shown: solvent exposure (grey), charged (red), polar (blue), hydrophobic (green), metal (dim grey). Hydrogen bonds are shown: to side chain atom (dotted arrow) and to backbone atom (full arrow). MD simulated structure is the average structure of the most populated cluster during MD simulations. Both ATP and Tyr-AMP acquire hydrogen bonds between main-chain of Val215 and adenine ring; Asn212 between 2'-OH group of ribose moiety. Lys154 from the CP1 insertion loop acquires hydrogen bond with γ -phosphate of ATP. The K⁺ ion (K₁⁺) was changed by another K⁺ ion (K₂⁺) during MD.

possible to observe such ordering (coiling) of this region in *BtTyrRS*^{ATP+Tyr} (Figure 3). The bacterial *Thermus thermophilus* TyrRS (*TtTyrRS*, PDB ID: 1H3E) (Yaremchuk et al., 2002) has also an analogous residue Arg93, which is close to γ -phosphate but does not form hydrogen bond with it. Probably such hydrogen bond forms only when Mg²⁺ coordinates all three phosphates of ATP providing appropriate triphosphate group conformation. Using the superposition method, we modeled several complexes of different aaRSs class Ic with the typical ATP conformation (Figure S3). In result, all complexes show similar ATP(P γ):(NH³⁺)Lys/Arg interaction from the opposite site of the catalytic loop. Moreover, mutation of analogous Arg86 in *GsTyrRS* R86A displays rate constants up to 8000 times lower comparing to the wild type enzyme (Fersht, Knill-Jones, Bedouelle, & Winter, 1988). Thus, an evolutionary conserved ATP(P γ):(NH³⁺)Lys/Arg interaction, like Lys154 in the CP1 disordered

region Val153–His158 of *BtTyrRS*, is one of the crucial interactions for the Tyr-AMP (Trp-AMP) formation in subclass Ic aaRSs.

For bacterial TyrRS on the base of crystal structures analysis, it was suggested that γ -phosphate of ATP can interact with the TyrRS without an interaction with the catalytic loop and contributes to the initial binding of the ATP molecule (Kobayashi et al., 2005). Therefore, Lys154 may play a similar role in case of mammalian TyrRS. We also noticed that different enzymes of class Ic aaRS may use different structural elements to interact with γ -phosphate (Figure S3). For instance, CP1 insertion does not interact with ATP in *TtTyrRS* while other loop is responsible for γ -phosphate binding. Interesting that interaction between Lys/Arg and γ -phosphate in mammalian TyrRS is more similar those in bacterial TrpRS and archaeal TyrRS, but not to bacterial TyrRS and human TrpRS (Figure S3).

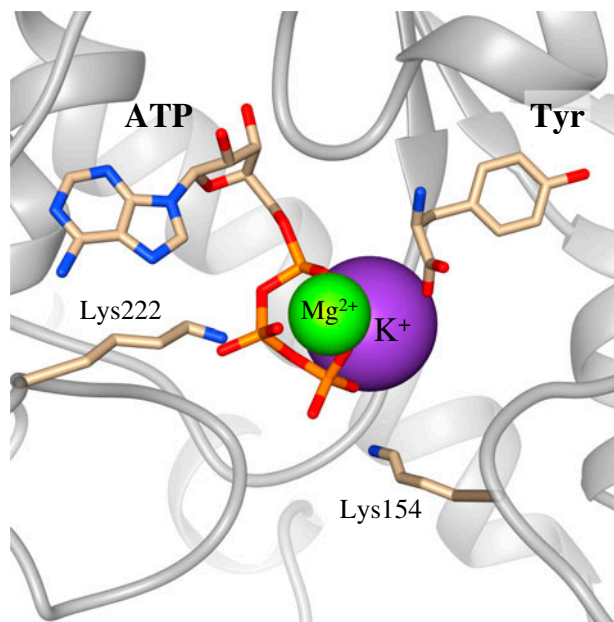


Figure 6. Typical binding of the lysine residues and ATP: Mg^{2+} into the active site of *BtTyrRS*. Lys222 (K^1) and Lys154 (CP1) bind phosphate groups of ATP in a clump manner. Mg^{2+} and K^+ ions are coordinating the electronegative groups of ATP (triphosphate group) and L-tyrosine (carboxyl group) substrates and bridge them keeping close to each other.

3.6. Interactions between the substrates and the ions into the active site

Earlier, significant domains' movement during L-tryptophan activation was shown for a bacterial TrpRS (Kapustina & Carter, 2006; Retailleau et al., 2003). Such movements of the anticodon binding and Rossmann-fold domains occur via hinge mechanism and bring the ATP and L-tryptophan together to form Trp-AMP (Kapustina & Carter, 2006; Retailleau et al., 2003). In contrast, such hinge-like domains' movement was not seen in TyrRS (Kobayashi et al., 2005) raising the question how two electronegative groups (triphosphate and carboxyl) of the substrates can be attracted one to another.

Analysis of our MD simulations data revealed that the Mg^{2+} and K^+ ions bring together ATP and L-tyrosine and bridge them (Figure 6). However, because of limitations of the MD simulation method (see Section 2.5), it is impossible to observe a chemical reaction. We even could not observe approaching of L-tyrosine (O_{T2}) and ATP (P_A) atoms on the covalent bond distance. Nevertheless, during our MD simulations, positively charged Mg^{2+} and K^+ were dragging negatively charged COO^- group of L-tyrosine to ATP's phosphate group (Video S2). As a result, the minimum distance detected between those pairs of atoms during whole MD simulations was 0.338 nm (initial distance

was 0.53 nm). Thus, such ion-bridging mechanism in mammalian TyrRS may be an analog of the hinge-like mechanism in bacterial TrpRS.

3.7. Dynamics of pre- and post- PP_i releasing state

Tyr-AMP and PP_i are products of the first step of catalytic reaction. MD simulation of *BtTyrRS*^{Tyr-AMP+ PP_i} was performed with the purpose to investigate factors leading to the PP_i release. It was also unknown whether Mg^{2+} and K^+ ions take part in the further catalysis or release with PP_i . For bacterial TyrRS, it was suggested that tRNA^{Tyr} CCA-acceptor triplet cannot reach the catalytic site without the removal of the KMSKS loop cover; the catalytic loop should adopt a semi-open conformation to allow such movements (Kobayashi et al., 2005).

Firstly, we carried out 100 ns MD simulations of the *BtTyrRS*_{Cm}^{Tyr-AMP+ PP_i} complex with compact KMSSS loop conformation. We expected that the loop would partially open with further PP_i releasing. However, both $PP_i:Mg^{2+}$ and K^+ have been remaining in the active site during the whole 100 ns MD simulation interval (Figures 7(A) and 7(C)). During the course of MD simulations, amino acid residues of the KMSSS and CP1 insertion loops were covering the PP_i . Such cover prevents its releasing. By comparing the starting structure and the structure after 100 ns of MD simulation, we noticed that the KMSSS residues shifted outward the active site for 0.36 nm. However, His49, Lys154, and Lys231 still held PP_i into the active site region (Figure 7(B)). Thus, despite that such partial opening had place to occur, it was not enough for PP_i releasing. In general, changing of conformation of the catalytic loop from the compact to the extended is quite possible since its "guiding" part (²²¹SKMSSEEEES²³⁰) is mostly composed of hydrophilic residues. Most likely, that at such stage of the catalytic reaction, the conformational change (opening) of the catalytic loop occurs in a large timescale since it is complicated by the presence of the intermediates. Therefore, we modeled the additional *BtTyrRS*_{Ex}^{Tyr-AMP+ PP_i} complex with the extended KMSSS loop conformation and produced its short (20 ns) MD simulations.

It was revealed that $PP_i:Mg^{2+}$, together with K^+ , were released rapidly (14 ns) from the active site when the KMSSS loop is in the extended conformation (Figures 7(A) and 7(C)). In the yeast TyrRS crystal (TyrRS[Tyr-AMP analogue] in complex with tRNA^{Tyr}) (PDB id: 2DLC), 10 residues of the catalytic loop (including KMSAS residues of the KMSKS motif) are missing (Tsunoda et al., 2007). It is important to note that the KMSAS loop in the yeast TyrRS is quite homological to the KMSSS loop in mammalian TyrRS; in the 2DLC crystal the yeast TyrRS active site contains Mg^{2+} ion

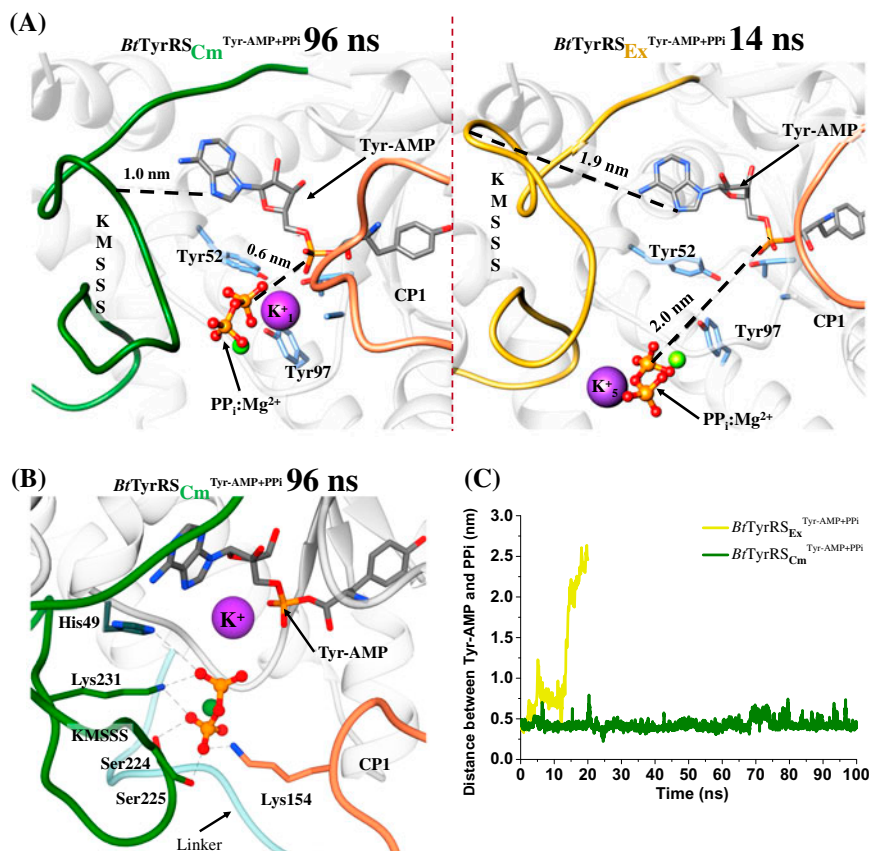


Figure 7. Dynamical behavior of *BtTyrRS* complexes with the Tyr-AMP, $\text{PP}_i\text{:Mg}^{2+}$ and K^+ ligands and different conformations of KMSSS loop. Van der Waals radii of K^+ and Mg^{2+} ions are decreased for clarity. A. The catalytic loops are in green (compact conformation) and yellow (extended conformation). The CP1 insertion is in coral. Despite that KMSKS motif has slightly shifted (0.36 nm) outwards the active site, $\text{PP}_i\text{:Mg}^{2+}$ has been remaining in the active site of *BtTyrRS*_{Cm}^{Tyr-AMP+PP_i} during 100 ns of simulation time. In the *BtTyrRS*_{Ex}^{Tyr-AMP+PP_i} complex $\text{PP}_i\text{:Mg}^{2+}$ rapidly (14 ns) has left the active site. Up to five K^+ ions took part in the PP_i releasing (see Video S3). Distances from Lys222 (K^1) to adenine ring are shown to ensure different states of catalytic loop. B. Another projection of the *BtTyrRS*_{Cm}^{Tyr-AMP+PP_i} at 96 ns frame. $\text{PP}_i\text{:Mg}^{2+}$ is covered by residues of the catalytic loop and the CP1 insertion loop, which prevent its releasing. Residues Thr42, Ala43, Tyr52 and Tyr97 (potassium-binding pocket) were coordinating K^+ ion. C. Graph shows distance between the Tyr-AMP and PP_i molecules as a function of time in *BtTyrRS*^{Tyr-AMP+PP_i} complexes with the different catalytic loop conformations. In case of *BtTyrRS*_{Ex}^{Tyr-AMP+PP_i} the distance is growing, indicating on the releasing of $\text{PP}_i\text{:Mg}^{2+}$ from the active site.

which is bounded in the exact same way as the K^+ ion in mammalian TyrRS (Figure S4). On the basis of our data, we suggest the following possible explanation why the catalytic loop is disordered while the TyrRS is bounded both to tRNA^{Tyr} and Tyr-AMP: the catalytic loop has the extended conformation and, therefore, is too flexible to be detected. Taking together, these observations suggest that after Tyr-AMP formation the KMSSS loop adopts the extended form. The extended form would allow the diphosphate releasing and following 3'-CCA terminus of tRNA^{Tyr} accessing to fully exposed Tyr-AMP. This suggestion supports similar hypothesis of the authors concerning the yeast TyrRS (Tsunoda et al., 2007). Further MD simulations of mammalian TyrRS in complex with tRNA^{Tyr} should reveal details of this process.

In the previous section, we mentioned that K^+ ions are attracted by the active site and can interchange. It is curious, that during MD simulation course $\text{PP}_i\text{:Mg}^{2+}$ interacts with different K^+ ions from the water-ion medium. These K^+ ions approach separately to $\text{PP}_i\text{:Mg}^{2+}$ dragging it away from the active site in a “step-by-step” manner (Video S3).

Comparing to other TyrRSs (bacterial and archaeal), the presence of the K^+ -binding pocket is inherent only for mammalian TyrRS. Moreover, in mammalian TyrRS the conservative $\text{H}^1\text{I}^2\text{G}^3\text{H}^4$ motif has meaningful substitution: H^4/Y^4 , where Y^4 (Tyr52) is a part of potassium-binding pocket (Figures 7(A) and 7(B)). Probably, these differences between mammalian and other TyrRSs' active sites may be used in designing of new inhibitors of “pathogenic” TyrRS. We also assume that such

mobility and van der Waals radius of K^+ ion (comparing to K^4) may weaken the binding of non-specific molecules (inhibitors of TyrRS of pathogenic organisms) to the mammalian TyrRS active site.

4. Conclusion

In this study, we constructed the complexes of *Bt*TyrRS with substrates and intermediates using the set of computational modeling techniques. To understand the dynamical features of each step of the catalytic reaction, several 100 ns of MD simulations for selected complexes were performed.

Analysis of MD trajectories revealed high flexibility of the catalytic KMSSS loop in the substrate-free state that could explain the absence of $^{222}KMSSEEE^{229}$ residues coordinates in crystal structures of mini-*Hs*TyrRS. However, at the presence of ATP and L-tyrosine substrates, the catalytic loop was keeping its compact conformation. Notably, the catalytic loop is quite different in bacterial and mammalian TyrRSs regarding sequence homology and conformational dynamics.

We analyzed interactions between the enzyme and ions/substrates/intermediates by comparing structural snapshots of initial and MD simulated *Bt*TyrRS complexes. Our data revealed *Bt*TyrRS[ATP] binding interactions and stable hydrogen bonds with Trp40, Asn212, Val215, Lys222, and namely Lys154, which is localized in the CP1 disordered region (Val153–His158) and probably plays a one of the key roles in ATP: Mg^{2+} binding. While the interaction between the γ -phosphate and Lys/Arg appears to be typical for class Ic aaRSs, our data suggest that the enzymes of different organisms may use different structural elements for realization of such bonding.

This work revealed the crucial role of Mg^{2+} and K^+ ions, which coordinate electronegative groups of ATP (phosphate groups) and L-tyrosine (carboxyl group) and probably compensate their electrostatic repulsion. We revealed that $PP_i:Mg^{2+}$, together with K^+ , rapidly left the active site when the catalytic loop had the extended conformation, emphasizing that namely the extended conformation is appropriate for 3'-CCA terminus of tRNA^{Tyr} entering.

Thus, using computational modeling we provided a wide-range of structural data for mammalian TyrRS. The set of different models has been uploaded on the Protein Structure Database of the MolDynGrid VL web-portal. This work will aid to the development of specific inhibitors for TyrRS of different pathogenic organisms. In addition, the structural data obtained are solid background for further *in silico* research of mammalian TyrRS complexes and its mutant forms associated with neurodegenerative diseases.

Supplementary material

The supplementary material for this paper is available online at <http://dx.doi.org/10.1080/07391102.2016.1235512>. The video files are available at the following links: Video_S1 – goo.gl/0QdRNt; Video_S2 – goo.gl/rF9yRi; Video_S3 – goo.gl/gBOeI3.

Abbreviations

aaRS	Aminoacyl-tRNA synthetase
ATP: Mg^{2+}	adenosine 5' triphosphate with Mg^{2+}
<i>Bt</i> TyrRS	<i>Bos taurus</i> tyrosyl-tRNA synthetase
<i>Bt</i> TyrRS _{Ex}	<i>Bt</i> TyrRS _{Cm} , <i>Bt</i> TyrRS ^{Tyr} , <i>Bt</i> TyrRS ^{ATP+Tyr} , <i>Bt</i> TyrRS _{Cm} ^{Tyr-AMP+PPi} , <i>Bt</i> TyrRS _{Ex} ^{Tyr-AMP+PPi} , see Table 1
CMT	Charcot–Marie–Tooth disorder
CP1	Connecting Polypeptide 1
<i>Gs</i> TrpRS	<i>Geobacillus stearothermophilus</i> TrpRS
<i>Hs</i> TrpRS	human TrpRS
<i>Hs</i> TyrRS	human TyrRS
$K^1 M^2 S^3$	
$K^4 S^5$	corresponding position in the KMSKS signature motif
MD	molecular dynamics
MD-simulated structure	average structure of the most populated cluster during MD simulations
<i>Mt</i> TyrRS	<i>Mycobacterium tuberculosis</i> TyrRS
PDB	Protein Data Bank
<i>Pf</i> TyrRS	<i>Plasmodium falciparum</i> TyrRS
PP _i	diphosphate ion
R_g	radius of gyration
RMSD	root mean square deviations
RMSF	root mean square fluctuations
TrpRS	tryptophanyl-tRNA synthetase
<i>Tt</i> TyrRS	<i>Thermus thermophilus</i> TyrRS
Tyr-AMP	tyrosyl-adenylate
TyrRS	tyrosyl-tRNA synthetase

Acknowledgements

Authors acknowledge Prof. M.A. Tukalo and Dr. S.O. Yesylevskyy for useful discussions, the administrators of Ukrainian National Grid-infrastructure for technical support and Ricardo O. S. Soares for the “readHBmap” python script.

Disclosure statement

No potential conflict of interest was reported by the authors.

Funding

This work was supported by State target scientific and technical program “Implementation and application of grid technologies 2009–2013”, by complex program of NAS of Ukraine “Grid-infrastructure and grid-technologies for scientific and prac-

tical-scientific applications 2014–2016” and by the EGI-Engage project (Horizon 2020 EU framework programme) [grant number 654142]. O.V. Savyt'skyi was supported by the YTF FEBS in 2010–2016, EBSA Bursary in 2013, Travel Grant from Cineca (IT) with PRACE (EU) in 2015 and Fellowship for Young Scientists from National Academy of Sciences of Ukraine (2012–2014, 2016–2017). V.V. Mykuliak was supported by the YTF FEBS in 2012–2015 and EBSA Bursaries in 2013–2015.

ORCID

Vladyslav O. Kravchuk  <http://orcid.org/0000-0001-9523-9089>
 Oleksandr V. Savyt'skyi  <http://orcid.org/0000-0002-8150-4416>
 Vasyl V. Mykuliak  <http://orcid.org/0000-0002-2522-9907>

References

- Abergel, C., Rudinger-Thirion, J., Giege, R., & Claverie, J. (2007). Virus-encoded aminoacyl-tRNA synthetases: Structural and functional characterization of mimivirus TyrRS and MetRS. *Journal of Virology*, *81*, 12406–12417.
- Austin, J., & First, E. (2002a). Comparison of the catalytic roles played by the KMSKS motif in the human and *Bacillus stearothermophilus* tyrosyl-tRNA synthetases. *Journal of Biological Chemistry*, *277*, 28394–28399.
- Austin, J., & First, E. (2002b). Potassium functionally replaces the second lysine of the KMSKS signature sequence in human tyrosyl-tRNA synthetase. *Journal of Biological Chemistry*, *277*, 20243–20248.
- Bedouelle, H. (1990). Recognition of tRNA^{Tyr} by tyrosyl-tRNA synthetase. *Biochimie*, *72*, 589–598.
- Bhatt, T., Khan, S., Dwivedi, V., Bandy, M., Sharma, A., Chandele, A., ... Craig, A. (2011). Malaria parasite tyrosyl-tRNA synthetase secretion triggers pro-inflammatory responses. *Nature Communications*, *2*, 530.
- Bjellmar, P., Larsson, P., Cuendet, M., Hess, B., & Lindahl, E. (2010). Implementation of the CHARMM force field in GROMACS: Analysis of protein stability effects from correction maps, virtual interaction sites, and water models. *Journal of Chemical Theory and Computation*, *6*, 459–466.
- Bonnefond, L., Giege, R., & Rudinger-Thirion, J. (2005). Evolution of the tRNA^{Tyr}/TyrRS aminoacylation systems. *Biochimie*, *87*, 873–883.
- Buddha, M., & Crane, B. (2005). Structures of tryptophanyl-tRNA synthetase II from *deinococcus radiodurans* bound to ATP and tryptophan: Insight into subunit cooperativity and domain motions linked to catalysis. *Journal of Biological Chemistry*, *280*, 31965–31973.
- Budiman, M., Knaggs, M., Fetrow, J., & Alexander, R. (2007). Using molecular dynamics to map interaction networks in an aminoacyl-tRNA synthetase. *Proteins: Structure, Function, and Bioinformatics*, *68*, 670–689.
- Bussi, G., Donadio, D., & Parrinello, M. (2007). Canonical sampling through velocity rescaling. *The Journal of Chemical Physics*, *126*, 014101.
- Chen, V., Arendall, W., Headd, J., Keedy, D., Immormino, R., Kapral, G., ... Richardson, D. (2009). MolProbity: All-atom structure validation for macromolecular crystallography. *Acta Crystallographica Section D: Biological Crystallography*, *66*, 12–21.
- Chen, D., Menche, G., Power, T., Sower, L., Peterson, J., & Schein, C. (2007). Accounting for ligand-bound metal ions in docking small molecules on adenylyl cyclase toxins. *Proteins: Structure, Function, and Bioinformatics*, *67*, 593–605.
- Chen, L., Wang, P., Dan-Jie, T., Tao, X., Man, R., Qiu, H., ... Zhu, H. (2016). Metronidazole containing pyrazole Derivatives potently inhibit tyrosyl-tRNA synthetase: Design, synthesis and biological evaluation. *Chemical Biology and Drug Design*, *88*, 592–598. doi:10.1111/cbdd.12793
- Datt, M., & Sharma, A. (2014). Conformational landscapes for KMSKS loop in tyrosyl-tRNA synthetases. *Journal of Structural and Functional Genomics*, *15*, 45–61.
- Daura, X., Gademann, K., Jaun, B., Seebach, D., van Gunsteren, W., & Mark, A. (1999). Peptide folding: When simulation meets experiment. *Angewandte Chemie International Edition*, *38*, 236–240.
- Doublé, S., Bricogne, G., Gilmore, C., & Carter Jr. C. (1995). Tryptophanyl-tRNA synthetase crystal structure reveals an unexpected homology to tyrosyl-tRNA synthetase. *Structure*, *3*, 17–31.
- Essmann, U., Perera, L., Berkowitz, M., Darden, T., Lee, H., & Pedersen, L. (1995). A smooth particle mesh Ewald method. *The Journal of Chemical Physics*, *103*, 8577–8593.
- Eswar, N., Webb, B., Marti-Renom, M., Madhusudhan, M., Eramian, D., Shen, M., ... Sali, A. (2006). Comparative protein structure modeling using modeller. *Current Protocols in Bioinformatics*, *15*, 5.6.1–5.6.30.
- Fersht, A., Knill-Jones, J., Bedouelle, H., & Winter, G. (1988). Reconstruction by site-directed mutagenesis of the transition state for the activation of tyrosine by the tyrosyl-tRNA synthetase: A mobile loop envelopes the transition state in an induced-fit mechanism. *Biochemistry*, *27*, 1581–1587.
- First, E., & Fersht, A. (1995). Analysis of the role of the KMSKS loop in the catalytic mechanism of the tyrosyl-tRNA synthetase using multimutant cycles. *Biochemistry*, *34*, 5030–5043.
- Fiser, A., Do, R., & Šali, A. (2000). Modeling of loops in protein structures. *Protein Science*, *9*, 1753–1773.
- Froelich, C., & First, E. (2011). Dominant intermediate Charcot-Marie-Tooth disorder is not due to a catalytic defect in tyrosyl-tRNA synthetase. *Biochemistry*, *50*, 7132–7145.
- Hanoian, P., Liu, C., Hammes-Schiffer, S., & Benkovic, S. (2015). Perspectives on electrostatics and conformational motions in enzyme catalysis. *Accounts of Chemical Research*, *48*, 482–489.
- Hess, B., Bekker, H., Berendsen, H., & Fraaije, J. (1997). LINCS: A linear constraint solver for molecular simulations. *Journal of Computational Chemistry*, *18*, 1463–1472.
- Humphrey, W., Dalke, A., & Schulten, K. (1996). VMD: Visual molecular dynamics. *Journal of Molecular Graphics*, *14*, 33–38.
- Jordanova, A., Irobi, J., Thomas, F., Van Dijk, P., Meerschaert, K., Dewil, M., ... Timmerman, V. (2006). Disrupted function and axonal distribution of mutant tyrosyl-tRNA synthetase in dominant intermediate Charcot-Marie-Tooth neuropathy. *Nature Genetics*, *38*, 197–202.
- Jorgensen, W., & Madura, J. (1983). Quantum and statistical mechanical studies of liquids. 25. Solvation and conformation of methanol in water. *Journal of the American Chemical Society*, *105*, 1407–1413.
- Kapustina, M., & Carter, C. (2006). Computational studies of tryptophanyl-tRNA synthetase: Activation of atp by induced-fit. *Journal of Molecular Biology*, *362*, 1159–1180.
- Kobayashi, T., Takimura, T., Sekine, R., Vincent, K., Kamata, K., Sakamoto, K., ... Yokoyama, S. (2005). Structural snapshots of the KMSKS loop rearrangement for amino acid activation by bacterial tyrosyl-tRNA synthetase. *Journal of Molecular Biology*, *346*, 105–117.

- Kornelyuk, A. (1998). Structural and functional investigation of mammalian tyrosyl-tRNA synthetase. *Biopolymers and Cell*, 14, 349–359.
- Kornelyuk, A., Klimenko, I., & Odynets, K. (1995). Conformational change of mammalian tyrosyl-tRNA synthetase induced by tyrosyl adenylate formation. *Biochem Mol Biol Int*, 35, 317–322.
- Kornelyuk, A., Tas, M., Dubrovsky, A., & Murray, J. (1999). Cytokine activity of the non-catalytic EMAP-2-like domain of mammalian tyrosyl-tRNA synthetase. *Biopolymers and Cell*, 15, 168–172.
- Li, T., Froeyen, M., & Herdewijn, P. (2008). Comparative structural dynamics of Tyrosyl-tRNA synthetase complexed with different substrates explored by molecular dynamics. *European Biophysics Journal*, 38, 25–35.
- Li, R., Macnamara, L., Leuchter, J., Alexander, R., & Cho, S. (2015). MD simulations of tRNA and aminoacyl-tRNA synthetases: Dynamics, folding, binding, and allostery. *International Journal of Molecular Sciences*, 16, 15872–15902.
- Marti-Renom, M., Stuart, A., Fiser, A., Sánchez, R., Melo, F., & Šali, A. (2000). Comparative protein structure modeling of genes and genomes. *Annual Review of Biophysics and Biomolecular Structure*, 29, 291–325.
- Morris, G., Goodsell, D., Halliday, R., Huey, R., Hart, W., Belew, R., & Olson, A. (1998). Automated docking using a Lamarckian genetic algorithm and an empirical binding free energy function. *Journal of Computational Chemistry*, 19, 1639–1662.
- Morris, G., Huey, R., Lindstrom, W., Sanner, M., Belew, R., Goodsell, D., & Olson, A. (2009). AutoDock4 and AutoDockTools4: Automated docking with selective receptor flexibility. *Journal of Computational Chemistry*, 30, 2785–2791.
- Mykuliak, V., Dragan, A., & Kornelyuk, A. (2014). Structural states of the flexible catalytic loop of *M. tuberculosis* tyrosyl-tRNA synthetase in different enzyme-substrate complexes. *European Biophysics Journal*, 43, 613–622.
- Naidenov, V., Vudmaska, M., Kornelyuk, A., & Matsuka, G. (2000). Site-directed mutagenesis of lysine residues located in the connection peptide of the nucleotide-binding domain (Rossmann fold) of tyrosyl-tRNA synthetase from bovine liver *Biopolymers and Cell*, 16, 275–280.
- Naidenov, V., Vudmaska, M., & Matsuka, G. (2001). Kinetic parameters of the tRNA^{Tyr} transcript aminoacylation by the bovine liver tyrosyl-tRNA synthetase. *Biopolymers and Cell*, 17, 534–539.
- Páll, S., Abraham, M., Kutzner, C., Hess, B., & Lindahl, E. (2015). Tackling exascale software challenges in molecular dynamics simulations with GROMACS. In S. Markidis, & E. Laure (Eds.), *Solving software challenges for exascale* (Vol. 8759, pp. 3–27). Stockholm: Springer International.
- Parrinello, M., & Rahman, A. (1981). Polymorphic transitions in single crystals: A new molecular dynamics method. *Journal of Applied Physics*, 52, 7182–7190.
- Pettersen, E., Goddard, T., Huang, C., Couch, G., Greenblatt, D., Meng, E., & Ferrin, T. (2004). UCSF chimera? A visualization system for exploratory research and analysis. *Journal of Computational Chemistry*, 25, 1605–1612.
- Retailleau, P., Huang, X., Yin, Y., Hu, M., Weinreb, V., Vachette, P., ... Ilyin, V. (2003). Interconversion of ATP binding and conformational free energies by tryptophanyl-tRNA synthetase: Structures of ATP bound to open and closed, pre-transition-state conformations. *Journal of Molecular Biology*, 325, 39–63.
- Sajish, M., & Schimmel, P. (2015). A human tRNA synthetase is a potent PARP1-activating effector target for resveratrol. *Nature*, 519, 370–373.
- Salnikov, A., Sliusar, I., Sudakov, O., Savytskyi, O., & Kornelyuk, A. (2009). MolDynGrid virtual laboratory as a part of Ukrainian Academic Grid infrastructure. *IEEE international workshop on Intelligent Data Acquisition and Advanced Computing Systems: Technology and Applications*, 2009, IDAACS 2009 (pp. 237–240). Cosenza: IEEE.
- Salnikov, A., Sliusar, I., Sudakov, O., Savytskyi, O., & Kornelyuk, A. (2010). Virtual laboratory moldyngrid as a part of scientific infrastructure for biomolecular simulations. *International Journal of Computing*, 9, 295–301.
- Savytskyi, O., & Kornelyuk, A. (2015). Computational modeling of molecular dynamics of G41R mutant form of human tyrosyl-tRNA synthetase, associated with Charcot-Marie-Tooth neuropathy. *The Ukrainian Biochemical Journal*, 87, 142–153.
- Savytskyi, O., Sliusar, I., Yesylevskyy, S., Stirenko, S., & Kornelyuk, A. (2011). Integrated tools for molecular dynamics simulation data analysis in the MolDynGrid virtual laboratory. *2011 IEEE 6th international conference on Intelligent Data Acquisition and Advanced Computing Systems (IDAACS)* (Vol. 1, pp. 208–211). Prague: IEEE.
- Savytskyi, O., Yesylevskyy, S., & Kornelyuk, A. (2013). Asymmetric structure and domain binding interfaces of human tyrosyl-tRNA synthetase studied by molecular dynamics simulations. *Journal of Molecular Recognition*, 26, 113–120.
- Sekine, S., Nureki, O., Dubois, D., Bernier, S., Chenevert, R., Lapointe, J., & Yokoyama, S. (2003). ATP binding by glutamyl-tRNA synthetase is switched to the productive mode by tRNA binding. *The EMBO Journal*, 22, 676–688.
- Shen, M., & Sali, A. (2006). Statistical potential for assessment and prediction of protein structures. *Protein Science*, 15, 2507–2524.
- Shen, N., Zhou, M., Yang, B., Yu, Y., Dong, X., & Ding, J. (2008). Catalytic mechanism of the tryptophan activation reaction revealed by crystal structures of human tryptophanyl-tRNA synthetase in different enzymatic states. *Nucleic Acids Res*, 36, 1288–1299.
- Starzyk, R., Webster, T., & Schimmel, P. (1987). Evidence for dispensable sequences inserted into a nucleotide fold. *Science*, 237, 1614–1618.
- Strom, A., Fehling, S., Bhattacharyya, S., & Hati, S. (2014). Probing the global and local dynamics of aminoacyl-tRNA synthetases using all-atom and coarse-grained simulations. *Journal of Molecular Modeling*, 20, 2245.
- Swiderek, K., Tunon, I., Moliner, V., & Bertran, J. (2015). Computational strategies for the design of new enzymatic functions. *Archives of Biochemistry and Biophysics*, 582, 68–79.
- Tsunoda, M., Kusakabe, Y., Tanaka, N., Ohno, S., Nakamura, M., Senda, T., ... Nakamura, K. T. (2007). Structural basis for recognition of cognate tRNA by tyrosyl-tRNA synthetase from three kingdoms. *Nucleic Acids Research*, 35, 4289–4300.
- Van Der Spoel, D., Lindahl, E., Hess, B., Groenhof, G., Mark, A., & Berendsen, H. (2005). GROMACS: Fast, flexible, and free. *Journal of Computational Chemistry*, 26, 1701–1718.
- Wakasugi, K., Quinn, C., Tao, N., & Schimmel, P. (1998). Genetic code in evolution: Switching species-specific aminoacylation with a peptide transplant. *The EMBO Journal*, 17, 297–305.
- Wakasugi, K., & Schimmel, P. (1999a). Highly differentiated motifs responsible for two cytokine activities of a split human trna synthetase. *Journal of Biological Chemistry*, 274, 23155–23159.

- Wakasugi, K., & Schimmel, P. (1999b). Two distinct cytokines released from a human aminoacyl-tRNA synthetase. *Science*, *284*, 147–151.
- Xiao, Z., Wei, W., Wang, P., Shi, W., Zhu, N., Xie, M., ... Zhu, H. (2015). Synthesis and evaluation of new tyrosyl-tRNA synthetase inhibitors as antibacterial agents based on a N2-(arylacetyl)glycinanilide scaffold. *European Journal of Medicinal Chemistry*, *102*, 631–638.
- Yang, X., Guo, M., Kapoor, M., Ewalt, K., Otero, F., Skene, R., ... Schimmel, P. (2007). Functional and crystal structure analysis of active site adaptations of a potent anti-angiogenic human tRNA synthetase. *Structure*, *15*, 793–805.
- Yang, X., Liu, J., Skene, R., McRee, D., & Schimmel, P. (2003). Crystal structure of an EMAP-II-Like cytokine released from a human tRNA synthetase. *Helvetica Chimica Acta*, *86*, 1246–1257.
- Yang, X., Otero, F., Skene, R., McRee, D., Schimmel, P., & Ribas de Pouplana, L. (2003). Crystal structures that suggest late development of genetic code components for differentiating aromatic side chains. *Proceedings of the National Academy of Sciences*, *100*, 15376–15380.
- Yang, X., Skene, R., McRee, D., & Schimmel, P. (2002). Non-linear partial differential equations and applications: Crystal structure of a human aminoacyl-tRNA synthetase cytokine. *Proceedings of the National Academy of Sciences*, *99*, 15369–15374.
- Yaremchuk, A., Kriklivyi, I., Tukalo, M., & Cusack, S. (2002). Class I tyrosyl-tRNA synthetase has a class II mode of cognate tRNA recognition. *The EMBO Journal*, *21*, 3829–3840.
- Yesylevskyy, S. (2015). Pteros 2.0: Evolution of the fast parallel molecular analysis library for C++ and python. *Journal of Computational Chemistry*, *36*, 1480–1488.
- Yesylevskyy, S., Savytskyi, O., Odynets, K., & Kornelyuk, A. (2011). Interdomain compactization in human tyrosyl-tRNA synthetase studied by the hierarchical rotations technique. *Biophysical Chemistry*, *154*, 90–98.
- Zoete, V., Cuendet, M., Grosdidier, A., & Michielin, O. (2011). SwissParam: A fast force field generation tool for small organic molecules. *Journal of Computational Chemistry*, *32*, 2359–2368.